Integrated Aeroservoelastic Tailoring of Lifting Surfaces

Thomas A. Zeiler*
PRC Kentron, Inc., Hampton, Virginia
and
Terrence A. Weisshaar†
Purdue University, West Lafayette, Indiana

An approach to the problem of simultaneous design of a structure and control law to meet aeroelastic stability objectives is presented. An idealized aeroelastic model is used; two different lifting surface restraint conditions are considered, one of which simulates an important feature of free flight. The problem of simultaneous design, called "integrated aeroservoelastic tailoring," is posed as an optimization problem to which is applied multilevel linear decomposition, dividing the aeroservoelastic system into structural and control subsystems. The system level objective is the minimization of a stability index to bring about stability of the system at a chosen airspeed, while the system is constrained to remain stable at lower airspeeds. The subsystem designs are constrained to be optimal in their respective senses through the use of optimal sensitivity derivatives with respect to specific design parameters. Application of this procedure is shown to produce optimally controlled structures with stability characteristics superior to those of open-loop and initial closed-loop designs. The results demonstrate both the difficulties and benefits of application of an integrated design procedure.

Introduction

THE design of an aerospace vehicle is a complex, multidisciplinary task requiring multiple interactions among the various disciplinary design groups involved. Most conventional design or optimization procedures are confined to a single discipline. In particular, active control seeks to improve (or even to "cure") structural dynamic design inadequacies often discovered "after the fact." While there is a recognized interrelationship between structural design and control synthesis, problems nonetheless arise in reconciling measures of performance. This can only add to the existing segregation of disciplinary design groups. While this segregation is understandable and somewhat justifiable, it need not be the blueprint for the future.

The products of each design group (e.g., planform, structure, control system, powerplant) interact in diverse ways when they are integrated into the final product—the flight vehicle. Future competition for a limited number of aerospace products will increase the desirability of accounting for these multidisciplinary interactions in the preliminary stages of design when configuration decisions are less firm. This will allow a fuller exploitation of emerging technologies, such as composite materials and active controls, that offer wider design options. In turn, increased creative interaction among the various disciplinary design groups will be required. Such a multidisciplinary approach to design is already under scrutiny for application to space structures.[1-8]

In this paper, an approach is suggested for the integration of two design activities, structural design and active control design. This integrated design process is referred to as "integrated aeroservoelastic tailoring." The use of the word "tailoring" anticipates the use of advanced composite construction in an actual wing design, although composite materials are not expressly considered in this study. To illustrate this approach, a highly idealized aeroservoelastic system is used. While the presentation focuses upon theory and models, the real emphasis of the presentation is an illustration of the dependency of the success of both disciplines upon each other's efforts. At the very least, it represents a technique that can be used as a departure point for a very real goal—the eventual integration of structural and control designs at an early stage of vehicle design.

Aeroservoelastic Model

The idealized aeroelastic model used for the present study is depicted in Fig. 1. It consists of two noninterfering airfoil elements attached to a rigid "fuselage" with freedom only in body pitch. One airfoil is attached to the fuselage by linear and rotational springs and includes a trailing edge control surface; the second airfoil, whose sole purpose is pitch stabilization, is rigidly attached to the fuselage element. The equations of motion for this idealization have the form[9]

$$M\ddot{x}+Kx=F_a \tag{1}$$

In this equation, M and K are mass and structural stiffness matrices and F_a a vector of motion-dependent aerodynamic loads. The four degrees of freedom shown in Fig. 1 are arranged in vector form as

$$x=\begin{Bmatrix} \theta \\ h/b=\tilde{h} \\ \alpha_e \\ \beta \end{Bmatrix}$$

Laplace transform methods are well suited to a stability study of Eq. (1). Such an approach relies upon the representation of the Laplace transform of aerodynamic loads computed in the frequency domain. The loads used in the present analysis are those originally developed by Theodorsen for a typical section airfoil,[10] with pitch, plunge, and control surface rotation degrees of freedom operating in incompressible

Presented as Paper 86-1005 at the AIAA/ASME/ASCE/AHS 27th Structures, Structural Dynamics and Materials Conference, San Antonio, TX, May 19-21, 1986; received April 24, 1986; revision received May 6, 1987.

*Project Structures Engineer. Member AIAA.
†Professor, School of Aeronautics and Astronautics. Associate Fellow AIAA.

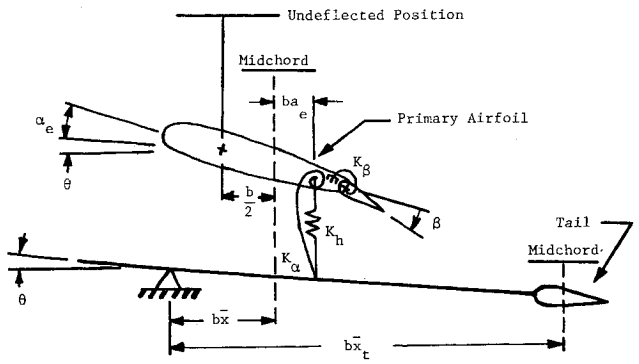

Fig. 1 4-degree-of-freedom aeroelastic model.

flow. These loads may be converted to the time domain through a Fourier synthesis procedure.[11] An exponential series approximation for the Wagner function,[12] expressed as

$$\phi(\bar{t}) = \sum_{i=1}^{N} a_i e^{b_i \bar{t}} \tag{2}$$

is then used in the superposition integral

$$I = \int_0^{\bar{t}} \frac{dQ}{d\bar{\tau}} \phi(\bar{t}-\bar{\tau}) d\bar{\tau} \tag{3}$$

that occurs in the time-domain loads expressions. In Eqs. (2) and (3), $\bar{t}$ and $\bar{\tau}$ are nondimensional time variables $[t = t(U/b)]$ and Q the upwash for the airfoil ¾ chord. The final result has the form of Roger's approximation,[13]

$$\bar{F}_a(\bar{s}) = q\left[\hat{A}_0 \bar{s}^2 + \hat{A}_1 \bar{s} + \hat{A}_2 + \sum_{m=1}^{\ell} \frac{\hat{B}_m \bar{s}}{\bar{s} + \bar{\gamma}_m}\right] \bar{x}(\bar{s}) \tag{4}$$

where $\bar{s}$ is the nondimensional Laplace variable and q the dynamic pressure. The $\hat{A}$ and $\hat{B}$ matrices are explicit functions of airfoil parameters and the a_i and b_i coefficients in Eq. (2). The so-called lags $\bar{\gamma}_m$ correspond to $-b_i$ in Eq. (2). Airfoil parameters were selected to match an airfoil studied by Edwards.[14,15] For the present study, the shear center position (denoted as the parameter a_e) will be used as a design parameter. Because of this, parameters normally defined with respect to the shear center are redefined with respect to the midchord, leaving mass properties unaffected by shear center position. The aerodynamic loads expression, derived for a three-degree-of-freedom airfoil, is converted for use in the four-degree-of-freedom model by applying a scaling factor together with load and coordinate transformations.[9] For the four-degree-of-freedom model, $\bar{x}_t = 10$ (see Fig. 1) and the nondimensional radius of gyration of the fuselage/tail with respect to the pivot is 10. With the representation of the airloads in Eq. (4), a state-space model of the system equations of motion can be formulated. The control surface equation of motion is modified by restricting the analysis to irreversible controls. The control deflection response β is related to a commanded input β_c through an actuator dynamic equation

$$a\ddot{\beta} + b\dot{\beta} + c\beta = \beta_c \tag{5}$$

This permits the state-space equations for the aeroservoelastic system to be written in the form

$$\dot{X} = AX + Bu \tag{6}$$

In Eq. (6), X is a state vector comprised of structural deflections and rates, the associated aerodynamic state vectors resulting from the representation in Eq. (4), and the control surface deflections and rates. The control vector u (a scalar in the present case) represents the commanded control β_c. The coefficients in Eq. (5) were chosen to match the uncoupled frequency (300 rad/s) of the trailing-edge control used by Edwards.[14,15] A detailed development and specifics of the A and B matrices used in this study is omitted here for brevity, but can be found in Ref. 9. This development is patterned after that found in Ref. 16.

Control Law Synthesis

The control law synthesis procedure for the present study uses steady-state linear-quadratic regulator (SSLQR) theory.[17] With SSLQR theory, a control is sought to minimize a quadratic function of system states X and the control u, subject to satisfaction of the equations of motion [Eq. (6)] viz.,

$$\min_u J = \int_0^{\infty} (y^* Q y + u^* R u) dt \tag{7a}$$

$$\text{STO: } \dot{X} = AX + Bu \tag{7b}$$

$$y = CX \tag{7c}$$

where the acronym STO is read "subject to" and the asterisk denotes Hermitian transpose. The output matrix C selects a combination of states in X to be included in the cost function J. For the present study, the matrix C is an identity matrix, but with those entries corresponding to the aerodynamic states set equal to zero. Thus, the aerodynamic states do not contribute to J. The weighting matrix for the outputs [Eq. (7c)] is Q, chosen to be an identity matrix, and the weighting on the control is R, chosen to be unity. The solution to the optimal SSLQR problem is a linear, full-state feedback control law

$$u = GX \tag{8a}$$

$$G = -R^{-1} B^* P \tag{8b}$$

where P is the minimum solution[18] to the steady-state matrix Riccati equation

$$PA + A^* P + C^* Q C - PBR^{-1} B^* P = 0 \tag{9}$$

Stability and Active Control Characteristics

Figure 2 shows the open-loop divergence and flutter boundaries of this model for a range of shear center positions a_e and the ratio of the tail semichord to the primary airfoil semichord b_t/b. Effects upon stability boundaries of aft/forward shear center positions resemble the wash-in/out effects of forward/aft wing sweep or similar effects of composite tailoring.[9,19-22] Note that as b_t/b increases, low-frequency body-freedom flutter is suppressed and the stability boundaries become those of the isolated flexible airfoil. Thus, this simple model displays much of the behavior observed in other studies of aircraft aeroelastic stability with pitch freedom.

Control laws to improve stability were obtained for the aircraft model (with $\bar{x} = 5.0$ and statically stable, but with no tail) for a range of shear center positions and values of nondimensional design airspeed $\bar{U}_{des}$ defined as $(U_{des}/b\omega_h)$. It should be pointed out that $\bar{U}_{des}$ is not an aircraft design airspeed but rather the airspeed chosen for control law synthesis. Figure 3 shows a contour plot of values of the minimized cost function J[Eq. (7a)] vs shear center position and design airspeed. The

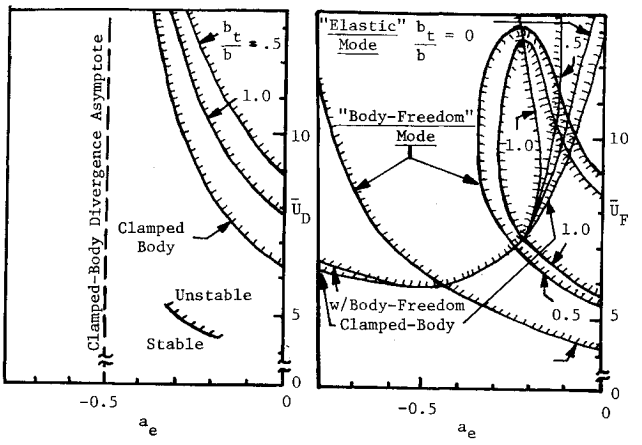

Fig. 2 Aircraft model open-loop stability boundaries; $\bar{x}_t = 10$, $\bar{x} = 5$: a) divergence, b) flutter.

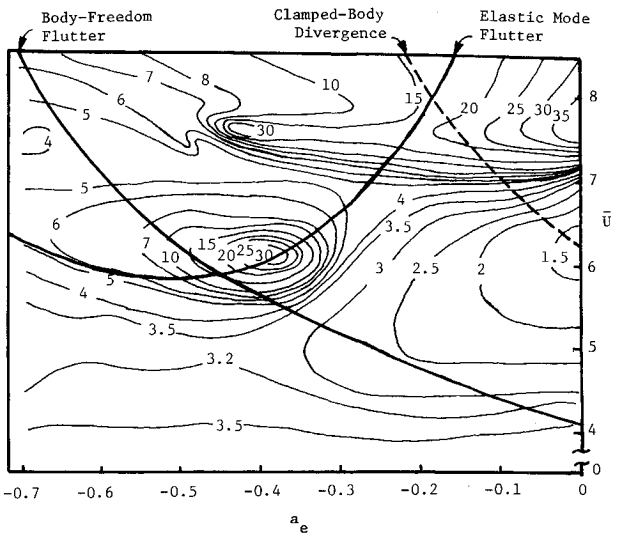

Fig. 3 Aircraft model control cost contours as functions of a_e and $\bar{U}_{des}$ (no tail, $\bar{x} = 5$).

evaluation of J is

$$J = X_0^* P X_0 \tag{10}$$

where P is the Riccati solution [Eq. (9)] and X_0 the initial condition on the state vector. For this initial condition, all initial states were chosen to be zero, except that $\alpha_e(0) = 0.1745$ rad and $\dot{\alpha}_e(0) = -0.07635$ rad/s. Also shown superimposed on Fig. 3 are the open-loop stability boundaries.

Figure 3 shows regions that represent "good" designs in the sense that J is relatively low. There are also regions of high cost near the points $(a_e, \bar{U}_{des}) = (-0.4, 6.0)$ and $(a_e, \bar{U}_{des}) = (-0.45 - 0.0, 7.0 - 8.0)$. These latter regions represent combinations of a_e and $\bar{U}_{des}$ for which the control synthesis experiences difficulty producing low-cost, stabilizing control laws.[18] This near instability (uncontrollability of unstable modes) can be visualized as proximity of open-loop poles (eigenvalues) to zeros of the loop transfer matrix.[14] This loop transfer matrix is defined as

$$TM(s) = C[Is - A]^{-1}B = N(s)/\Delta(s) \tag{11}$$

This equation can be obtained by combining the Laplace transforms of Eqs. (7b) and (7c) to get

$$\bar{y}(s) = TM(s)\bar{u}(s) \tag{12}$$

In Eq. (11), $\Delta(s)$ represents the characteristic polynomial of A. Poles are roots of $\Delta(s)$, while zeros are those values of s that make an element of $N(s)$ zero.

Figure 4 shows pole and zero "migrations" that occur with changes in airspeed when the shear center position is at $a_e = -0.4$. The values $s = N_z$ ($z = \theta, \tilde{h}$, or α_e) denote zeros for which the control has no observable influence upon the output z. Figure 4 shows that θ, $\tilde{h}$, and α_e zeros cluster around the "elastic" mode flutter poles (in the root locus labelled "bending") near $\bar{U} = 6.0$. This point corresponds to one of the cost peaks in Fig. 3. There is also proximity of $\tilde{h}$ and α_e zeros to the body-freedom flutter mode poles (in the root locus labelled "pitch"). The first of these proximities is associated with stabilization difficulties with the high-frequency flutter mode and the second with the body-freedom flutter mode.

When the body pitch degree-of-freedom is eliminated, near instability of the high-frequency or "classical" flutter mode remains a problem, as is seen from the cost contour plot in Fig. 5. This occurs because the characteristics of the high-frequency elastic mode flutter are relatively unaffected by lower-frequency body modes. However, the second high-cost region is quite different. Pole-zero plots presented in Ref. 9 but not shown here show proximity of zeros to divergence poles for the corresponding values of a_e and $\bar{U}_{des}$. This cost peak and the elongated region in Fig. 3 are clearly related, as are the instabilities of airfoil divergence and body-freedom flutter, such as those found in Ref. 20.

Although the areas of low cost in Figs. 3 and 5 indicate "good" control designs from the standpoint of SSLQR theory, they do not necessarily indicate desirable designs from the standpoint of overall system aeroelastic stability. Consider Fig. 6, which shows *closed-loop stability boundaries* of the *actively controlled* airfoil model and open-loop stability boundaries. This figure was constructed by fixing $\bar{U}_{des}$ to be 6.0 and then determining an optimal SSLQR control law for each of a large number of selected values of a_e. Within a certain range of a_e values, the control laws were successful in extending the upper part of the flight envelope. However, near $a_e = 0.0$, divergence occurs *below* the open-loop divergence speed. Figure 5 shows that J is relatively low in this region. For shear center positions forward of the midchord, active control provides little benefit even though, as guaranteed by SSLQR theory, the system is stabilized *at* $\bar{U} = \bar{U}_{des}$. Similar plots[9] for designs speeds of 5.5 and 6.5 show similar undesirable off-design stability characteristics, even though all J values for $\bar{U}_{des} = 5.5$ are quite low. *This indicates that the design cost function J from SSLQR theory is inadequate as a sole performance index for use in an integrated design process where the aircraft must be stable up to* $\bar{U}_{des}$.

Design Procedure for Aeroservoelastic Tailoring

In view of the previous results, an integrated design procedure based upon multilevel linear decomposition,[23,24] was developed and implemented with a maximum stable airspeed as the overall system design objective. This was accomplished in a sequential fashion by stabilizing the system through structural and control redesign at successively higher airspeeds while maintaining stability at lower airspeeds.

A set of airspeeds $\bar{U}_j$ is selected with $\bar{U}_k$ denoting the lowest of these selected airspeeds for which the system is unstable. The immediate tailoring objective is then written in the form of an optimization problem for seeking the minimum value of the "objective" stability index F_{sk} (to be defined later) associated with the "objective" airspeed $\bar{U}_k$,

$$\min_{y,u} F_{sk} \tag{13a}$$

$$\text{STO:} \quad F_{sj} < 0 \quad \text{for all} \quad \bar{U}_j < \bar{U}_k \tag{13b}$$

control is optimal

$$J_c = \min_u J_c^{(u)} \tag{13c}$$

$$g_c(u) \tag{13d}$$

structure is optimal

$$J_s = \min_y J_s(y) \tag{13e}$$

$$g_s(y) \tag{13f}$$

The structural design variables are represented by y, while u represents control variables. The system is constrained to be stable at all $\bar{U}_j$ below $\bar{U}_k$. The objective functions J_c and J_s are constrained to be minima for the control and structural optimizations and g_c and g_s are associated constraints. Since the immediate objective is stability at $\bar{U}_k$, the minimum of F_{sk} is only sought, not necessarily obtained.

The method of multilevel linear decomposition,[23,24] wherein a multidisciplinary system is decomposed into smaller monodisciplinary subsystems, was applied to the present aeroservoelastic system to create control and structural subsystems. The disciplinary design variables y and u are determined by the subsystem optimizations performed individually and, largely, independently while certain parameters are held fixed. These parameter p_i may be explicit or implicit functions of the design variables. At the integrated level, where the optimal control and structure are recombined, these parameters become design variables and are changed to achieve system-level objectives. These parameter changes are returned to the disciplinary design groups where the subsystems are reoptimized for the new values of the parameters. For instance, if the integrated design asks for a new fundamental wing bending frequency, the structural design group reoptimizes the wing design variables (skin thicknesses, fiber angles, etc.) to match the requested frequency at minimum weight. However, the effects of the parameter changes upon the optimal subsystem designs, and ultimately the overall system, must be accounted for so that the parameter changes at the integrated level can be properly determined. This accounting is accomplished through the use of optimal sensitivity derivatives.[25] These derivatives tell the integrated design how the optimal design of each subsystem will change as the parameters p_i change. For the present work, the control design is obtained through optimal SSLQR synthesis. Since the structural model is so idealized, the structural subsystem design is not considered; however, structural parameters are used at the integrated system level. This implicitly assumes that there is never any cost or penalty (weight or otherwise) associated with changes in the structural parameters. For composite structures, this may not be unrealistic in certain cases.[26]

The optimization problem for the decomposed system, using optimal sensitivity derivatives of the stability indices, is now written (NP is the number of parameters)

$$\min_{\Delta p} F_{sk} \approx F_{sk0} + \sum_{i=1}^{NP} \frac{\partial F_{sk}}{\partial p_i} \Delta p_i \tag{14a}$$

$$\text{STO:} \quad F_{sj} \approx F_{sj0} + \sum_{i=1}^{NP} \frac{\partial F_{sj}}{\partial p_i} \Delta p_i < 0$$

$$\text{for all} \quad \bar{U}_j < \bar{U}_k \tag{14b}$$

$$J_c = \min_u J_c(u) \tag{14c}$$

$$g_c(u) \tag{14d}$$

$$p_i^{\ell} \le p_i \le p_i^{u}, \quad i = 1 \to \text{NP} \tag{14e}$$

$$\Delta p_i^{\ell} \le \Delta p_i \le \Delta p_i^{u}, \quad i = 1 \to \text{NP} \tag{14f}$$

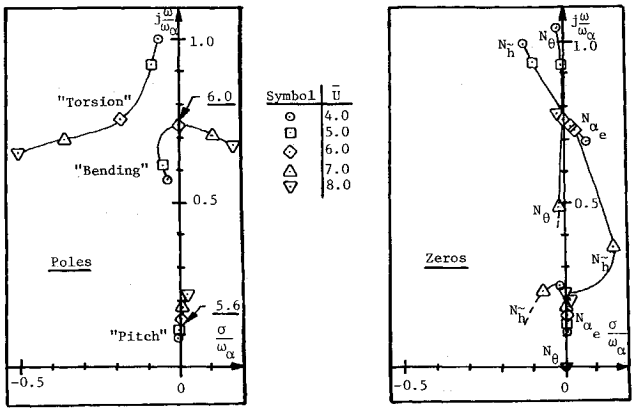

Fig. 4 Poles and zeros of aircraft model loop transfer matrix (no tail, $\bar{x} = 10$, $a_e = -0.4$).

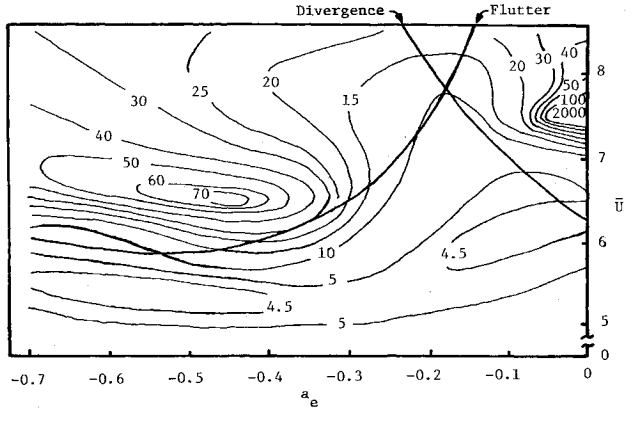

Fig. 5 Aircraft model control cost contours as functions of a_e and $\bar{U}_{des}$.

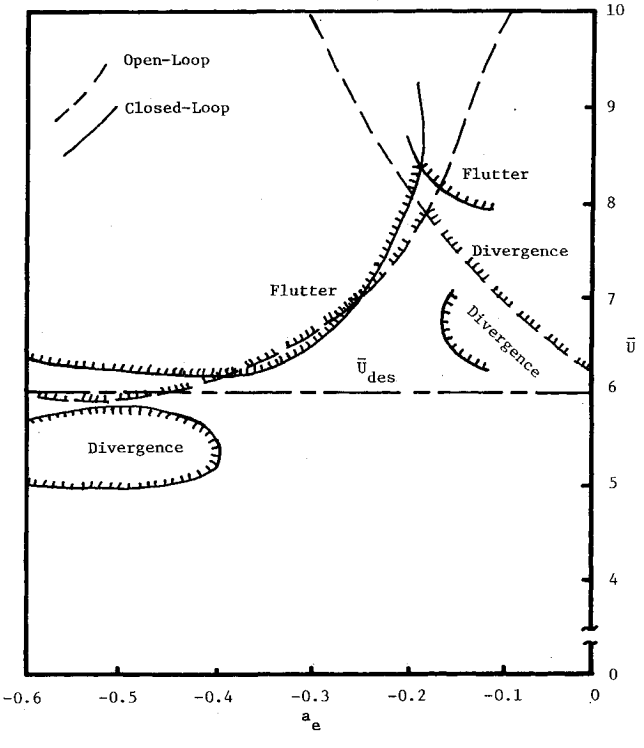

Fig. 6 Open- and closed-loop stability boundaries vs a_e for airfoil model.

The objective, Eq. (14a), is to select the changes in the design parameters that will produce the largest decrease in F_{sk} without violating the constraints. Equation (14b) expresses the constraint that the system must remain stable at all airpseeds below $\bar{U}_k$. Equations (14c) and (14d) express the subsystem optimality constraint implicitly satisfied by the use of optimal sensitivity derivatives. Equation (14e) represents side constraints on the parameters, and Eq. (14f) represents move limits to protect against excessive errors resulting from the linearization of the problem and to aid convergence. Because the objective function and constraints are assumed to be linear functions, the optimum parameter changes can be determined through a simplex-type procedure.[27] If parameter changes over several cycles are observed to be negligible, the process is assumed to have converged. If the process has not converged, the parameter changes are incorporated into the system definition and a new design cycle begins.

The stability index is given by the function

$$F_{sj} = \frac{1}{\rho} \ell n \left(\sum_{i=1}^{N} e^{\rho \sigma_i} \right) \tag{15}$$

where σ_i represents the real part of the ith system eigenvalue of a set of N system eigenvalues evaluated at airspeed $\bar{U}_j$ and ρ is a scaling parameter (chosen as unity). Useful characteristics of this function are continuity of its derivatives and boundedness. It can be shown that

$$\sigma_{i_{\max}} \leq F_{sj} \leq \sigma_{i_{\max}} + (1/\rho) \ell n(N) \tag{16}$$

The stability index is bounded from below by the maximum value of σ_i occurring in the set of N values of σ_i. The upper bound is determined by both ρ and N. Thus, a negative value of F_{sj} guarantees a stable system at $\bar{U}_j$. A positive F_{sj} will be taken to indicate an unstable system, although this is not always true.

To use the optimization procedure outlined, derivatives of the stability indices with respect to design parameters are required. The derivatives have the form

$$\frac{\partial F_s}{\partial p} = \sum_{i=1}^{N} e^{\rho \sigma_i} \frac{\partial \sigma_i}{\partial p} \Big/ \sum_{i=1}^{N} e^{\rho \sigma_i} \tag{17}$$

where

$$\frac{\partial \sigma_i}{\partial p} = \mathrm{Re} \left(\frac{\partial \lambda_i}{\partial p} \right) \tag{18}$$

and λ_i is an eigenvalue (in general complex) of the system. For the eigenvalue derivative,

$$\frac{\partial \lambda_i}{\partial p} = \{r_i\}^* \left[\frac{\partial A_+}{\partial p} \right] \{e_i\} \tag{19}$$

where r_i and e_i are the so-called left and right eigenvectors of the control-augmented system matrix A_+ for the eigenvalue λ_i. The control-augmented system matrix is defined as

$$A_+ = A + BG \tag{20}$$

where G is the optimal feedback gain matrix. So, for $B \neq B(p)$,

$$\frac{\partial A_+}{\partial p} = \frac{\partial A}{\partial p} + B \frac{\partial G}{\partial p} \tag{21}$$

Derivatives of G require derivatives of the Riccati solution P so that $[R \neq R(p)]$:

$$\frac{\partial G}{\partial p} = -R^{-1} B^* \frac{\partial P}{\partial p} \tag{22}$$

The Riccati equation constitutes a necessary condition for the optimal SSLQR solution. Differentiating it allows the solution for $\partial P/\partial p$ to be obtained from[28]

$$\frac{\partial P}{\partial p}[A - BR^{-1}B^*P] + [A - BR^{-1}B^*P]^* \frac{\partial P}{\partial p} + \left[P \frac{\partial A}{\partial p} + \frac{\partial A^*}{\partial p} P + \frac{\partial C^* Q C}{\partial p} - P \frac{\partial B R^{-1} B^*}{\partial p} P \right] = 0 \tag{23}$$

Equation (23) is a Lyapunov equation. In the present problem, B, C, Q, and R are independent of p. Thus, the optimal sensitivity derivatives of the stability indices describe how the stability indices of the *optimally controlled structure* should change with a change in the design parameter p.

Aeroservoelastic Tailoring Examples

The procedure described was applied to both the "isolated" three-degree-of-freedom airfoil model and the pitch-free four-degree-of-freedom "aircraft" model. Figure 7 shows the design-cycle histories for the isolated airfoil. In this example, F_{sj}, a_e, and $\bar{U}_{\text{des}}$ are shown for each cycle. For simplicity, only integer values of airspeed were selected for constructing the stability indices; the j subscripts correspond to these nondimensional airspeed values (e.g., F_{s7} is evaluated at $\bar{U}=7$). The initial design point was chosen to be $(a_e, \bar{U}_{\text{des}}) = (-0.4, 6.0)$, and the initial objective (maximum) airspeed was $\bar{U}=7$. The design procedure is seen to cause an initial increase in a_e (i.e., the shear center moves aft) to increase flutter speed. In addition, $\bar{U}_{\text{des}}$ decreases to avoid the troublesome divergence region visible in Fig. 6. This divergence region does not exist at lower values of $\bar{U}_{\text{des}}$.[9] At cycle 2, the design is driven toward a second divergence region, visible in the right portion of Fig. 6. However, at lower values of $\bar{U}_{\text{des}}$, this region is considerably larger.[9] The procedure avoids this divergence region by increasing $\bar{U}_{\text{des}}$ until the system is stabilized up to $\bar{U}=7$. At this point, stability up to and including $\bar{U}=8$ becomes the new objective. At cycle 5, the design procedure encounters a second flutter mode (visible in Fig. 6) and must restabilize the system at $\bar{U}=7$ by shifting the shear center slightly forward again. By cycle 7, the system is stabilized at both $\bar{U}=7$ and $\bar{U}=8$, making stability at $\bar{U}=9$ the new objective. The system cannot be stabilized at $\bar{U}=9$; however, F_{s9} is minimized when the procedure is halted at cycle 11. Figure 8 shows estimates obtained for the next cycle, although the parameter changes were not incorporated into the design. The end result of these 11 design cycles is that $\bar{U}_{\text{des}}$ is virtually unchanged from its initial value but the shear center is moved aft to $a_e = -0.189$. This result compares favorably with the results shown in Fig. 6. Pole/zero migrations with airspeed are shown in Fig. 8 for the initial design ($a_e = -0.4$) and for $a_e = -0.2$ (close to the final design). The structural redesign is seen to have improved the closed-loop stability characteristics by eliminating a stability problem with the flutter mode. In Fig. 8b, the troublesome mode is stabilized, and the N_α is moved far into the left half-plane, thus eliminating pole-zero proximity. Figure 9 depicts the closed-loop root loci for the initial and final designs. The final design is seen to be a compromise between flutter in two different modes.

Four-Degree-of-Freedom Example

The tailoring procedure was also applied to a statically stable four-degree-of-freedom aircraft model with no tail sur-

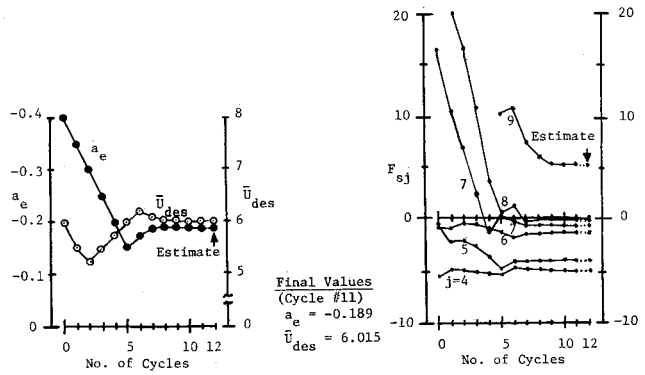

a) b)

Fig. 7 Design-cycle history; airfoil model: a) design parameters, b) stability indices.

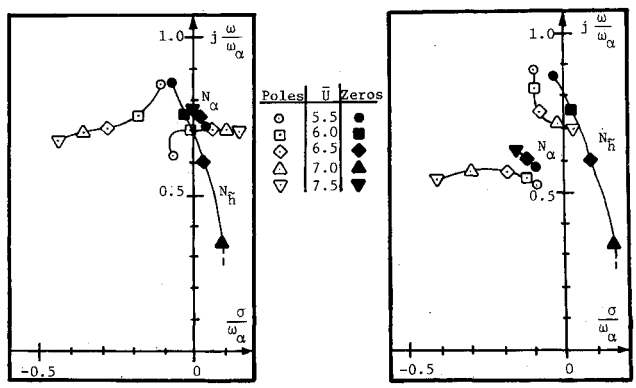

a) b)

Fig. 8 Poles and zeros of airfoil model loop transfer matrix: a) $a_e = -0.4$, b) $a_e = -0.2$

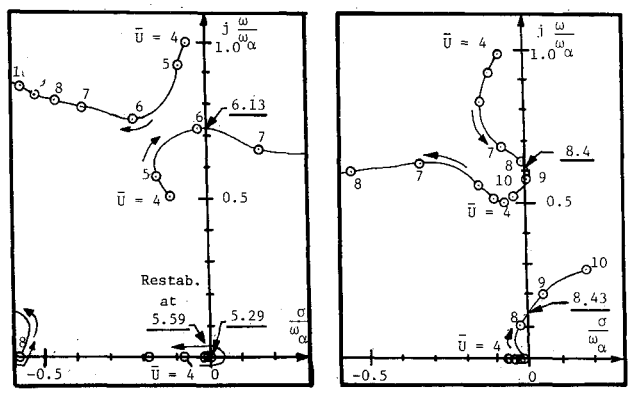

a) b)

Fig. 9 Closed-loop velocity root locus diagrams for airfoil model design: a) initial design, b) final design.

face. The Q and R weighting matrices used in Eq. (10a) for the previous study were arbitrarily chosen to be identity matrices. SSLQR theory requires the user to adjust the elements of these matrices to obtain improved control laws. These Q and R matrix elements may have a significant effect on the results of the control law synthesis and, in some cases, a poor choice can lead to the appearance of subcritical instabilities.[9] Accordingly, Q_θ (the weighting on the body pitch angle) was added to the list of control design parameters. The nondimensional position of the airfoil midchord with respect to the pivot point, denoted as $\bar{x}$, was also added to the list of structural configuration design parameters.

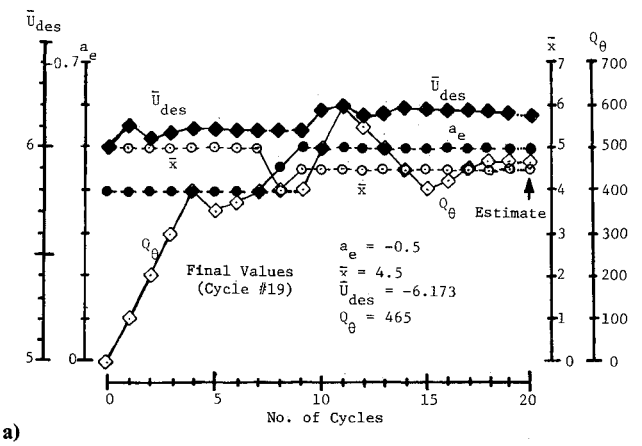

a)

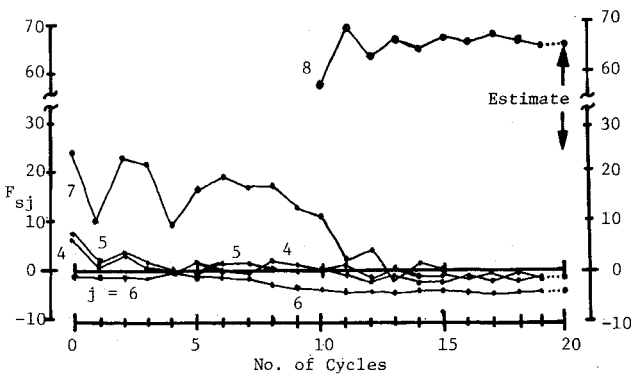

b)

Fig. 10 Design-cycle history; aircraft model: a) design parameters, b) stability indices.

Figure 10 shows the design-cycle histories that result for this idealized aircraft model. The initial objective was to stabilize the system at $\bar{U}=4$ and 5 using only the control design parameters $\bar{U}_{des}$ and Q_θ. The initial design points were taken to be $(a_e,\bar{x})=(-0.4,5.0)$ and $(\bar{U}_{des},Q_\theta)=(6.0,1.0)$. After design cycle 4, the procedure began to experience difficulty meeting objectives. As a result, through cycles 8 and 9, the control parameters $\bar{U}_{des}$ and Q_θ were held fixed, while the structural parameters were allowed to change. At cycle 12, the system was stable up to $\bar{U}=6$, making $\bar{U}=7$ the new objective airspeed. By cycle 16, the system was stable up to $\bar{U}=7$, making $\bar{U}=8$ the new objective airspeed. No further stabilization was possible by cycle 19, so the procedure was stopped. Further structural modification might have been pursued, but important effects of structural modification upon control design have been demonstrated. Figure 11 shows the partial derivatives of the stability indices with respect to Q_θ plotted against the design cycle number. Figure 11 indicates that changes in a_e and $\bar{x}$ during cycles 8 and 9 increased the magnitudes of $\partial F_{s4}/\partial Q_\theta$ and $\partial F_{s5}/\partial Q_\theta$, thus making Q_θ more effective in stabilizing the system at $\bar{U}=4$ and 5. Figure 4 shows the pole-zero migrations of the initial configuration with airspeed. The proximity of the zeros to the flutter poles near $\bar{U}=6$ reflects the difficulties encountered during the early design cycles. Figure 12 shows the pole-zero migrations for the modified structure. Unlike the isolated airfoil example, structural changes did not serve to stabilize the flutter pole for the aircraft model. In fact, the open-loop flutter speed was decreased when these changes occurred. However, structural changes did separate the zeros from the flutter poles, indicating enhanced controllability.

Root loci for the initial and final designs are shown in Fig. 13. The initial root loci show that the instabilities encountered

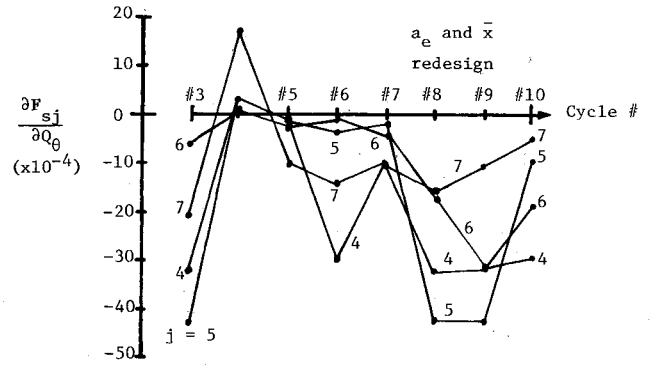

Fig. 11 $\partial F_{sj}/\partial Q_\theta$ vs design-cycle number; aircraft model.

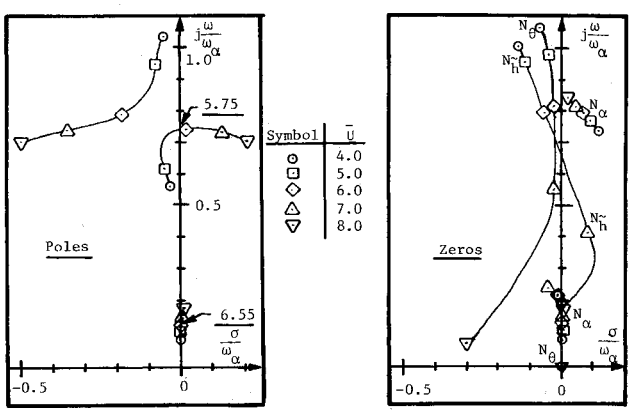

Fig. 12 Poles and zeros of aircraft model loop transfer matrix (no tail, $\bar{x}=4.5$, $a_e=-0.5$).

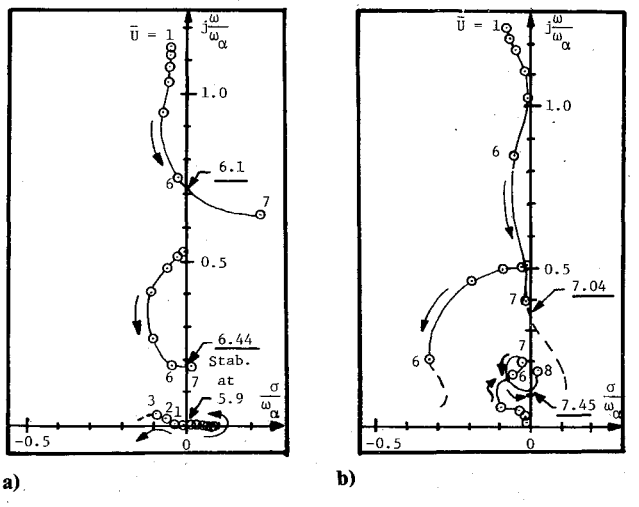

Fig. 13 Closed-loop velocity root locus diagrams for aircraft model designs: a) initial design, b) final design.

at $\bar{U}=4$ and 5 are divergence instabilities introduced by the active control being designed under conditions of near-uncontrollability. The root loci for the final design show it to be a compromise between flutter at $\bar{U}=7.04$ and flutter in a "hump" mode near $\bar{U}=5$.

Conclusion

Integrated aeroservoelastic tailoring may be accomplished by a number of approaches, one of which is presented in this paper. This approach has the advantage of preserving identities of the disciplinary design activities while achieving an integrated multidisciplinary design that takes account of the significant, meaningful interactions between subsystems. The specific examples presented demonstrate two possible beneficial effects of structural modifications upon control design. Structural changes can passively stabilize unstable modes that are nearly uncontrollable. On the other hand, structural modification may also enhance the controllability of these modes. It was also shown that the measure of control design optimality is not necessarily an adequate measure of desirability of the overall system performance, making integral design considerations that much more important.

Although the present work has used highly idealized modeling elements, it has shown that the optimization of an aeroservoelastic system can be done for the benefit of all participants. Studies using models with theoretical refinements such as finite-element wing structure modeling with provision for composites, nonzero Mach number, random loading, input/output noise, measurement feedback, and reduced-order controllers (to list but a few) should certainly be pursued. Also, consideration should be given to alternate design objectives. Such detailed studies can serve to further define the potential benefits (and limitations) of integrated aeroservoelastic tailoring.

Acknowledgments

This research was supported by NASA/Langley Research Center Grant NAG-1-157; Mr. J.R. Newsom was grant monitor. The authors gratefully acknowledge helpful discussions with Professors D.K. Schmidt and D.R. Andrisani and with Mr. M.G. Gilbert. Finally, while nobly encouraging "cross-talk" between disciplines, the authors may have unwittingly excluded significant references to simultaneous design. Such exclusions are not intentional.

References

[1]Hale, A.L. and Lisowski, R.J., "Optimal Simultaneous Structural and Control Design of Maneuvering Flexible Spacecraft," *Proceedings of 4th VPI & SU/AIAA Symposium on Dynamics and Control of Large Structures,* Blacksburg, VA, edited by L. Meirovitch, June 1983.

[2]Hale, A.L., Lisowski, R.J., and Dahl, W.E., "Optimizing Both the Structure and Control of Maneuvering Flexible Spacecraft," Paper presented at AAS/AIAA Astrodynamics Conference, Lake Placid, New York, Aug. 1983.

[3]Salama, M., Hamidi, M., and Demsetz, L., "Optimization of Controlled Structures," *Proceedings of Workshop on Identification and Control of Flexible Space Structures,* San Diego, CA, June 1984.

[4]Khot, N.S., Venkayya, V.B., and Eastep, F.E., "Structural Modifications of Large Flexible Structures to Improve Controllability," AIAA Paper 84-1906, Seattle WA, Aug. 1984.

[5]Khot, N.S., Eastep, F.E., and Venkayya, V.B., "Optimal Structural Modifications to Enhance the Optimal Active Vibration Control of Large Flexible Structures," AIAA Paper 85-0627, Orlando, FL, April 1985.

[6]Haftka, R.T., Martinovic, Z.N., and Hallauer, W.L. Jr., "Enhanced Vibration Controllability by Minor Structural Modifications," *AIAA Journal,* Vol. 23, Aug. 1985, pp. 1260–1266.

[7]Venkayya, V.B. and Tischler, V.A., "Frequency Control and Its Effect on the Dynamic Response of Flexible Structures," *AIAA Journal,* Vol. 32, Nov. 1985, pp. 1768–1774.

[8]Weisshaar, T.A., Newsom, J.R., Zeiler, T.A., and Gilbert, M.G., "Integrated Structure/Control Design—Present Methodology and Future Opportunities," ICAS Paper 86-4.8.1, Sept. 1986.

[9]Zeiler, T.A., "An Approach to Integrated Aeroservoelastic Tailoring for Stability," Ph.D. Thesis, School of Aeronautics and Astronautics, Purdue University, West Lafayette, IN, Aug. 1985.

[10]Theodorsen, T., "General Theory of Aerodynamic Instability and the Mechanism of Flutter," NACA TR-496, May 1934.

[11]Dowell, E.H., Curtis, H.C. Jr., Scanlan, R.H., and Sisto, F., *A Modern Course in Aeroelasticity,* Sijthoff and Noordhoff, Alphen aan Rijn, the Netherlands, 1980.

[12]Dowell, E.H., "A Simple Method for Converting Frequency-Domain Aerodynamics to the Time Domain," NASA TM-81844, Aug. 1980.
[13]Roger, K.L., Hodges, G.E., and Felt, L., "Active Flutter Suppression—A Flight Test Demonstration," *Journal of Aircraft,* Vol. 12, June 1975, pp. 551-556.
[14]Edwards, J.W., "Unsteady Aerodynamic Modeling and Active Aeroelastic Control," Stanford University, Stanford, CA, Rept. SUDDAR 504 (NASA Grant NGL-005-020-007), Feb. 1977, (available as NASA CR-148019).
[15]Edwards, J.W., "Unsteady Aerodynamic Modeling for Arbitrary Motions," *AIAA Journal,* Vol. 15, April 1977, pp. 593-595.
[16]Mukhopadhyay, V., Newsom, J.R., and Abel, I., "A Method for Obtaining Reduced-Order Control Laws for High-Order Systems Using Optimization Techniques," NASA TP-1876, Aug. 1981.
[17]Kailath, T., *Linear Systems,* Prentice-Hall, Englewood Cliffs, NJ, 1980.
[18]Martensson, K., "On the Matrix Riccati Equation," *Information Sciences,* Vol. 3, Jan. 1971, pp. 17-49.
[19]Weisshaar, T.A. and Foist, B.L., "Vibration and Flutter of Advanced Composite Lifting Surfaces," AIAA Paper 83-0961, 1983.
[20]Weisshaar, T.A., Zeiler, T.A., Hertz, T.J., and Shirk, M.H., "Flutter of Forward Swept Wings, Analyses and Tests," AIAA Paper 82-0646, May 1982.
[21]Niblett, L.T., "Divergence of Flutter of Swept-Forward Wings with Cross-Flexibilities," Royal Aircraft Establishment, London, TR-80047, April 1980.
[22]Weisshaar, T.A. and Zeiler, T.A., "Dynamic Stability of Flexible Forward Swept Wing Aircraft," *Journal of Aircraft,* Vol. 20, Dec. 1983, pp. 1014-1020.
[23]Sobieszczanski-Sobieski, J., James, B., and Dovi, A., "Structural Optimization by Multilevel Decomposition," *AIAA Journal,* Vol. 23, Nov. 1985, pp. 1775-1782 (see also AIAA Paper 83-0832).
[24]Sobieszczanski-Sobieski, J., "A Linear Decomposition Method of Large Optimization Problems—Blueprint for Development," NASA TM-83-248, February 1982.
[25]Sobieszczanski-Sobieski, J., Barthelemy, J.F., and Riley, K.M., "Sensitivity of Optimum Solutions to Problem Parameters," *AIAA Journal,* Vol. 20, Sept. 1982.
[26]Krone, N.J. Jr., "Divergence Elimination with Advaned Composites," AIAA Paper 75-1009, Aug. 1975.
[27]Fox, R.L., *Optimization Methods for Engineering Design,* Addison-Wesley, Reading, MA, 1971.
[28]Gilbert, M.G., "Design Parameter Sensitivity Methods in Optimal LQG Control Law Synthesis," AIAA Paper 85-1930, Aug. 1985.